CGU HS Committee on River Ice Processes and the Environment
16th Workshop on River Ice
Winnipeg, Manitoba, September 18 - 22, 2011

Satellite SAR Observations of River Ice Cover: A RADARSAT-2 (C-band) and ALOS PALSAR (L-band) Comparison

J.J. van der Sanden and H. Drouin
Natural Resources Canada, Canada Centre for Remote Sensing
588 Booth Street, Ottawa, Ontario K1A 0Y7
sanden@nrcan.gc.ca hudrouin@nrcan.gc.ca

In this paper we discuss the importance of microwave wavelength in terms of the interaction of microwaves with river ice cover and demonstrate its effect through combined analysis of RADARSAT-2 data (C-band, 5.55 cm nominal wavelength), ALOS PALSAR data (L-band, 23.62 cm nominal wavelength), and ground reference data for ice covers found in the Middle Channel of the Mackenzie River at Inuvik. The operating wavelength of a given SAR system governs its depth of penetration and affects its sensitivity to surface roughness and the presence of volume scatterers (e.g. air bubbles in the case of river ice). Our results show that RADARSAT-2, thanks to its shorter operating wavelength, offers more potential for the classification of river ice cover types than ALOS PALSAR. The HV-polarisation represents the best performing linear polarisation but performs less well than selected polarimetric variables. Both RADARSAT-2 and ALOS PALSAR backscatter measurements are found to make rather weak predictors of river ice cover thickness. To a large degree this is due to the very strong effect of ice structure on radar backscatter.

1. Introduction

River ice affects natural processes and human activities and therefore represents a significant component of the environment in northern countries like Canada. Information on river ice cover supports science, engineering and management activities including: hydraulic modelling, break-up forecasting, ice road routing, industrial water intake / discharge, hazard management, and wildlife management. River ice cover variables of interest typically include: coverage, type, thickness, and condition. Synthetic Aperture Radar (SAR) satellites make potentially outstanding tools for collecting up-to-date information on river ice thanks to their capability to routinely and systematically image extensive remote areas independent of weather and daylight conditions. During winter, when the ice is frozen solid, SAR satellites offer sensitivity to the physical structure of ice because radar waves will penetrate 'dry' ice cover and interact with features that define its internal properties.

In this paper we will discuss the results of a study into the potential of RADARSAT-2 and ALOS PALSAR for the mapping of ice cover characteristics in the Middle Channel of the Mackenzie River at Inuvik, NWT. The SAR images applied were acquired early April 2009 and are complemented with a set of ground reference data collected in February / March of 2009. RADARSAT-2 and ALOS PALSAR operate with C- and L-band microwaves, respectively. The effects of this large in difference operating frequency/wavelength on image information content and, as such, on potential for rive ice mapping will be discussed in this paper. Earlier findings regarding the application potential of RADARSAT-2 have been presented in van der Sanden *et al*. (2009) and van der Sanden and Drouin (2011).

2. Radar Image data and Interaction Basics

Table 1 lists the RADARSAT-2 and ALOS PALSAR data applied in this study. The principal difference between the two SAR satellites that acquired these data relates to their operating frequency and, by extension, operating wavelength. RADARSAT-2 operates in C-band at a frequency of 5.405 GHz and a wavelength of 5.55 cm while ALOS PALSAR operates in L-band at a frequency of 1.270 GHz and a wavelength of 23.62 cm. When travelling in ice (at -5° C) rather than free space, the wavelengths of the microwaves transmitted by RADARSAT-2 and ALOS PALSAR are reduced to about 3.11 cm and 13.24 cm, respectively. As shown in Table 1, there is a secondary difference between the data sets studied, that is, their angle of incidence differs by about 10 degrees. Fortunately, backscatter modelling results presented by Fung (1994, p. 398) show that the effect of frequency on backscattering behaviour of multi-year sea ice, that is, sea ice free of salt and thus similar to freshwater ice, is stronger than the effect of incidence angle.

The wavelength (λ) of the microwaves used to image fresh water ice, or any other target, governs the manner in which the incident microwaves interact with the target and generate backscatter. Specifically, the wavelength affects the depth of penetration and defines the effective surface roughness of scattering boundaries (e.g. ice / water interface) as well as the effective size of scattering particles in volumes (e.g. air bubbles).

The penetration depth of microwaves into a medium is proportional to their wavelength and the cosine of their angle of incidence (θ_{inc}) (e.g. Ulaby *et al.*, 1982). According to Mätzler and Wegmüller (1987) the penetration depth, at a 35° incidence angle, into ice nearly free of impurities (e.g. salts, air bubbles) and a temperature of -5° C by microwaves with wavelengths equivalent to RADARSAT-2 and ALOS PALSAR is about 14 m and 55 m, respectively. Due to the steeper incidence angle, the depth of penetration associated with the ALOS PALSAR data used in this study would be even larger. Lower temperatures reduce the absorption of microwave power by the ice and thus increase the depth of penetration. In contrast, an increase in saline impurities enhances microwave absorption and therefore decreases the penetration depth. The overall effect of an increase in air bubbles on microwave penetration depth is a function of their effective shape, size, and orientation. On the one hand, increased air content reduces microwave absorption and thus enhances penetration depth. On the other hand, however, air bubbles of a certain, wavelength dependent, size, shape and orientation may scatter incident microwave power in directions away from their original travel path and thus decrease the depth of penetration.

The effective surface roughness of a scattering boundary can be defined as its roughness relative to the wavelength of the incident microwaves. Similarly, the effective size of particles that make up a scattering volume represents their size relative to the wavelength of the incident microwaves. The effective surface roughness and the effective scatterer size govern the spatial distribution of scattered microwave power and, as such, the amount of microwave power scattered back towards the radar sensor, i.e. the radar return signal or backscatter. It should be noted that a surface corresponding to the boundary between two media will only generate (back)scatter if the media have different dielectric properties. Similarly, a particle in a certain volume will not (back)scatter unless its dielectric properties are different from those of its surroundings. In the case of winter ice cover, scattering occurs at both the air / ice and the ice / water interface. However, due to a larger dielectric contrast between ice and water than between air and ice, the ice / water interface, and its corresponding roughness, has a much stronger effect on the radar backscatter than the air / ice interface (cf. Gherboudj *et al*., 2010).

The scale of the roughness of a horizontal randomly rough surface can be characterized using the standard deviation of the surface height irregularities (h) or, in other words, the standard deviation of the differences between the actual (measured) surface heights and the mean (reference) surface height. As a rule of thumb, h is calculated from measurements with a horizontal spacing $\leq 0.1\lambda$ (Ulaby *et al*., 1982). Based on h, Sabins (1996) defines three effective roughness classes:

- Smooth ; $$h < \frac{\lambda}{25\cos(\theta_{inc})}$$ [1]

- Rough ; $$h > \frac{\lambda}{4.4\cos(\theta_{inc})}$$ [2]

- Intermediate ; $$\frac{\lambda}{4.4\cos(\theta_{inc})} \leq h \leq \frac{\lambda}{25\cos(\theta_{inc})}$$ [3]

Effectively smooth, intermediate, and rough surfaces that correspond to dielectric discontinuities can be expected to generate low, moderate, and strong backscatter levels, respectively. Table 2 defines the effective roughness for both the air / ice and ice / water interface of an ice cover imaged by RADARSAT-2 and ALOS PALSAR at an incidence angle of 35°. At an incidence angle of 24°, that is, the incidence angle of the ALOS PALSAR data applied in this study the defining numbers for *h* are 1.03 cm and 5.88 cm for the air / ice interface, and 0.58 cm and 3.29 cm for the ice / water interface. The difference in the effective roughness for both interfaces is explained by the difference in the velocity, and thus wavelength, of microwaves travelling in air versus ice. The values in Table 2 reflect the high sensitivity of microwaves to surface roughness.

As indicated earlier, the scattering behaviour of individual particles that may be present in the ice volume (e.g. air bubbles, liquid water pockets) depends strongly on their effective size and, for non-spherical particles, their shape and orientation. The effective size (χ) of a spherical particle is commonly expressed by the ratio of its circumference to the incident wavelength ($\chi = \pi d / \lambda$, where *d* stands for diameter). Depending on its effective size χ the behaviour of a spherical scatterer falls in one of three scattering regions which are typically defined as:

- Rayleigh (or low-frequency) scattering	;	$\chi < 0.1$	[4]
- Optical (or high-frequency) scattering	;	$\chi > 10$	[5]
- Mie (or resonant) scattering	;	$0.1 \leq \chi \leq 10$	[6]

Optical scattering is also known as geometric scattering or non-selective scattering. The scattering behaviour of a non spherical particle (e.g. cylinder, disc) will also fall within one of these three general regions but will vary as a function of its shape and orientation and, moreover, the polarization of the incident microwaves.

In the case of Rayleigh scattering, the illuminated particle is much smaller than the incident wavelength and initiates a single scattering process. Due to its larger effective size, a Mie scattering particle brings about multiple scattering processes that originate from different parts of its surface. Depending on the size of the particle, these scattering processes interfere in a constructive or destructive manner which produces a resonant or periodic variation in the scattered wave intensity. The scattering process of microwaves incident on an optical scatterer, i.e. a dielectric particle of a size much larger than the wavelength, resembles that of microwaves incident on an extended surface. Relative to Rayleigh scattering and Optical scattering, scattering in the Mie region is more difficult to predict/model as it is much more sensitive to variability in the scatterer's size and orientation. Unlike Mie and Optical scattering, Raleigh scattering does not usually generate much radar backscatter. In fact, Raleigh scattering tends to absorb microwave energy and thus lower the level of radar backscatter (Ulaby *et al*., 1981).

Table 3 shows the limits in terms of the diameter for a given spherical dielectric particle enclosed in ice, for both the RADARSAT-2 and ALOS PALSAR wavelengths, to exhibit a scattering behaviour that agrees with the three scattering regimes identified above. According to Gherboudj *et al*. (2007) the spherical air bubbles commonly found in frazil ice and snow ice have diameters ranging from about 0.1 cm to 0.5 cm and 0.001 cm to 1.2 cm, respectively. It follows that the scattering behaviour of frazil ice when observed by RADARSAT-2 will typically fall in the Mie scattering region. When observed by ALOS PALSAR, on the other hand, frazil ice will typically

behave as a Raleigh scattering target. The large variability in terms of the diameter of air bubbles in snow ice typically causes it to scatter conform either a Rayleigh or Mie scattering target both in the case of RADARSAT-2 and ALOS PALSAR.

In the practice, a radar system does not observe individual scattering particles but rather a collection of scatterers which may vary in terms of size, shape, orientation, and/or dielectric constant. Therefore, the radar backscatter measurements of e.g. ice rarely expose the particular, and potentially extreme, scattering behaviour of specific individual scattering particles. Instead radar systems will measure the backscatter contribution of the hypothetical effective scatterer which will be a function of its structural and material characteristics as well as volume fraction and spatial distribution.

The above text provides a basic understanding of the interaction of microwaves with fresh water ice as a function of wavelength and is intended to support the interpretation of the results presented in section 4. Readers interested in furthering their knowledge re the interaction of microwaves with river ice and how this may be implemented in a radar backscatter model are referred to the paper by Gherboudj *et al*. (2010).

3. Study Area and Ground Reference Data

The area of interest for the present study is the Mackenzie River near Inuvik, i.e. a section of the Middle Channel from Point Separation in the South to Oniak Island in the North (see Figure 1). The process of river freeze-up typically commences in early October and is a function of local meteorological and hydrodynamic factors as well as freeze-up events which occurred weeks earlier at distant upstream locations (Mackay, 1967). Sherstone (1984) reports an average maximum ice thickness for the Middle Channel of 104.5 cm for the winters of 1982 and 1983. Frequent formation of snow ice during the spring season due to flooding and refreezing is reported in Sherstone (1986).

Ground reference data were collected in the period from February 27 to March 9 of 2009 at 22 locations along the Middle Channel. These locations are believed to represent a good sample of the different ice covers found within the area of interest. They were pre-selected based on visual analysis of a RADARSAT-2 image acquired in January 2009. At each location, the characteristics of both the ice cover and snow cover were described in terms of snow/ice surface roughness, snow depth, snow grain size/type, snow hardness, snow dielectric properties, total ice thickness, and ice cover composition. Data on ice cover composition, i.e. ice type and thickness of composite ice layers, were obtained through laboratory analysis of extracted ice cores. Figure 2 visualizes the ground truth information collected at 5 locations. The backscattering behaviour of the corresponding ice / snow covers will be discussed in section 5 of this paper. From a radar remote sensing perspective, the most important difference between the three main ice types, that is, columnar ice, frazil ice, and snow ice relates to their variability in terms of air bubble and impurities (e.g. sediments) content. The volume fraction of these dielectric discontinuities typically increases going from columnar ice to frazil ice to snow ice.

Core 4-D represents a consolidated ice cover, i.e. a thick, porous and rough-surfaced accumulation of ice floes that was formed during freeze-up following the collapse of an initial

ice cover. Unlike the other cores, core 8-B was extracted from a lake rather than from the river. This core is special in the sense that it corresponds to a location were, over the course of the winter, the ice cover has grown to the lake bed. As such, this ice cover is not underlain by water but rather frozen ground. Given the distinct difference in the dielectric properties of frozen ground and water, the backscattering behaviour of ground-fast ice can be expected to differ from that of ice underlain by water. The formation of ground-fast ice is not limited to lakes but can also occur in river channels. Our approach of visual image analysis followed by fieldwork revealed considerable potential for confusion between ground-fast ice and snow covered dry river bed (ground). As such, an evaluation of the backscattering behaviour of the latter was also included in our analysis. Unfortunately, the site corresponding to core 8-B was not imaged by ALOS PALSAR.

The river ice thicknesses measured on all sites visited ranged from 70 cm to 145 cm, with the latter thickness corresponding to the consolidated ice cover found at site 4-D. The thickness of the sampled snow covers ranged from about 11 cm to 53 cm. At many locations, the snow cover included a layer of ice.

4. Data Analysis

The SAR image analysis approach involved the following steps for both the RADARSAT-2 and ALOS PALSAR data:

1) conversion of the single look complex RADARSAT-2 image and the three-look complex ALOS PALSAR image to the Kennaugh image format (assuming reciprocity and applying a Gamma look-up table).
2) generation of corresponding incidence angle images.
3) orthorectification of individual Kennaugh and incidence angle images to the UTM NAD 83 coordinate system (using nearest neighbour resampling and an output pixel spacing of 5 m by 5 m for RADARSAT-2 and 10 m by 10 m for ALOS PALSAR).
4) extract averaged Kennaugh matrix elements as well as average incidence angle values for pre-defined image regions, that is, image regions corresponding the fieldwork locations (ranging in size from 400 to 667 pixels for RADARSAT-2 and from to 104 to 160 pixels for ALOS PALSAR).
6) use extracted data to compute selected non-polarimetric and polarimetric variables for analysis, e.g. backscatter in various linear and circular polarisations, polarisation ratios, polarisation phase difference, polarisation coherence, Pauli decomposition elements, Freeman decomposition elements, Cloude and Pottier decomposition elements, and Touzi decomposition elements.

5. Results and Discussion

Scattering behaviour

Figure 3a and 3b show backscatter return signals measured in selected polarisations by, respectively, RADARSAT-2 and ALOS PALSAR at sites 3-B, 3-D, 4-D, 8-B, and 5-D (cf. Figure 2). The associated coding represents the make up of the ice core in terms of ice type (C = columnar, F = frazil, S = snow) and thickness in cm; for example the code F37_C51 for site 3-D indicates that this ice cover is comprised of 37 cm of frazil ice on top of 51 cm of columnar ice.

In terms of polarization: H = horizontal, V = vertical, R = right circular, L = left circular, TP = the total backscattered power. The first letter identifies the transmit polarisation while the second letter refers to the receive polarisation.

In the case of columnar ice (site 3-B), for both RADARSAT-2 and ALOS PALSAR, we observe relatively high responses in the HH-, VV-, and RL-polarisations and relatively low responses in the HV-, RR- and LL-polarisations. As discussed in section 3, the radar backscatter of columnar ice which is largely free of dielectric discontinuities originates primarily from surface scattering at the ice / water interface. Interestingly, the HH backscatter is shown to be larger but similar to the VV backscatter for RADARSAT-2, and larger than the VV backscatter for ALOS PALSAR. This pattern can also be observed for sites 3-D and 4-D. In fact, an evaluation of the complete data set shows that this holds true for all sites studied. By using additional RADARSAT-2 data for sites 3-B, 3-D, and 4-D, we show in Figure 4 that this pattern is rather persistent over the winter season, i.e. November 8 and onwards. In Geldsetzer *et al*. (2011) and van der Sanden and Drouin (2011) the ratio of the backscatter in VV and HH was already identified as a good indicator of the onset of freeze-up. The HH and VV backscatter behaviour observed in this study is not in agreement with results presented by Leconte *et al*. (2009) and Gherboudj *et al.* (2010). The results presented by the latter authors are consistent with observations from soil surfaces which show that the backscatter in HH and VV is similar at incidence angles up to about 20° and that the HH backscatter is lower (by several dB) than the VV backscatter at incidence angles over 20°. Further study is required to come up with a reasonable explanation for the observed deviant HH and VV backscatter behaviour. At this point in time we do know that the ice covers studied here are much less homogeneous than those studied/modelled by Leconte *et al.* (2009) and Gherboudj *et al.* (2010). Firstly, the characteristics of the ice covers found in the study area often vary significantly over short distances. Therefore, despite our best efforts to pick homogeneous sites, the image regions used for data extraction may include ice of varying properties. Secondly, our ice covers are overlain by a complex snow cover that typically includes a layer of ice.

The RADARSAT-2 and ALOS PALSAR backscatter measurements for site 3-D agree with the discussion in section 2 regarding the effective size of volume scattering particles and scattering regions. In the case of ALOS PALSAR, the presence of frazil ice was anticipated to induce Rayleigh scattering and result in lower backscatter levels. Indeed, the ALOS PALSAR backscatter levels for site 3-D, that is, a combination of frazil ice and columnar ice are lower than those for the columnar ice cover found at site 3-B. The total thickness of the ice covers at both sites is about the same. In the case of RADARSAT-2, again relative to columnar ice (site 3-B), the presence of frazil ice can be seen to create a large increase in HV, RR, and LL backscatter. The effective size of the bubbles contained in the frazil ice volume is sufficiently large to cause the incident RADARSAT-2 microwaves to reflect multiple times and generate relatively strong backscatter responses in HV, RR, and LL. Compared to columnar ice, frazil ice shows weaker radar return signals in the HH-, VV-, and RL-polarisation.

For both RADARSAT-2 and ALOS PALSAR and in all polarisations, the consolidated ice cover corresponding to site 4-D can be seen to create levels of backscatter that are much higher than those measured for columnar ice (site 3-B) or frazil ice (site 3-D). This ice cover has a very rough air/ice interface and, quite likely, a very rough ice/water interface and comprises multiple

layers consisting of different ice types. In addition to the air bubbles enclosed in the frazil and snow ice layers, this ice cover can be expected to include dielectric discontinuities such as air pockets, liquid water pockets, and cracks that will vary widely in size, shape, and orientation. Due to its complex structure, this ice cover enhances both surface scattering and volume scattering. The former leading to strong radar return signals in HH-, VV-, and RL-polarisation and the latter to high levels of backscatter in the HV-, RR-, and LL-polarization.

The ice core extracted at site 8-B contains both snow ice and columnar ice. However, the principal difference between site 8-B and, for example, site 3-B or 3-D relates to the fact that the ice at this location does not superimpose water but rather frozen ground. The dielectric contrast between ice and frozen ground is much smaller than the dielectric contrast between ice and water. As such, groundfast ice can be expected to induce less surface scattering and generate less backscatter than floating ice in HH, VV, and RL in particular. In the case of site 8-B, this reduction in backscatter from surface scattering can be expected to be partly compensated by increased volume scattering resulting from the presence of snow ice. With respect to the backscatter in HV, RR, and LL, the nature of the medium underlying the ice is of importance because it affects the level of backscatter resulting from interaction between volume scattering particles and the medium's surface. Figure 3b does not include the backscatter responses for site 8-b because the site was not imaged by ALOS PALSAR.

As evidenced in Figure 3 by the relatively high responses in HH, VV, and RL and the relatively low responses in HV, RR, and LL the backscatter behaviour of dry snow (site 5-D) is dominated by surface scattering rather than volume scattering. The snow – ground interface represents a much larger dielectric discontinuity than the snow – air interface and will therefore be the main (back)scattering surface. The RADARSAT-2 HH, HV, VV, TP, and RL backscatter responses for snow are lower than those for the groundfast ice found at site 8-B. This suggests potential for discriminating between the two targets. However, a reduced backscatter contrast should be expected between snow and groundfast ice that doesn't include a snow ice layer.

Ice type classification

Figure 5 summarizes the ice cover classification potential for a series of non-polarimetric and polarimetric variables as computed from the RADARSAT-2 and ALOS PALSAR data. The measure of classification potential shown assumes the use of a single band and is equal to the ratio of the coefficient of variation between the columnar ice class, merged frazil / snow ice class, and consolidated ice class, and the sum of the coefficients of variation within these three classes. The potential for classification will be higher when the between class coefficient of variation is large and the sum of the within class coefficients of variation is small, i.e. when the value of the measure shown in Figure 5 is high. Ground-fast ice and snow covered ground were excluded from this preliminary classification potential analysis.

In terms of classification potential, Figure 5 illustrates that RADARSAT-2 typically offers more potential than ALOS PALSAR. It can be shown that ALOS PALSAR is less suited for discrimination between columnar ice and frazil / snow ice in particular. This can be explained from its longer wavelength which makes it less sensitive to the air bubbles that define the difference between these two types of ice. The variables $|\alpha|^2$, $|\beta|^2$, and $|\gamma|^2$ and represent the single bounce (or odd-bounce), double bounce (or even-bounce), and volume scattering component of

the Pauli decomposition (Lee and Pottier, 2009). The even-bounce component computed from RADARSAT-2 can be seen to offer the best potential to differentiate between the ice classes studied. In decreasing order, for both RADARSAT-2 and ALOS PALSAR, the classification potential level of the three linear polarisation combinations ranks as HV, VV, and HH. The RR and LL polarization combination, notably for RADARSAT-2, perform better than the three linear polarization combinations. It can be seen that the ratioing of different polarizations does not improve the potential for classification.

Ice thickness estimation

Figure 6 summarizes the potential of non-polarimetric and polarimetric variables computed from RADARSAT-2 and ALOS PALSAR for the estimation of ice cover thickness. The coefficients of determination (R^2) for a linear regression between ice thickness and the different radar measurements are shown. Data points associated with ground-fast ice, snow on ground, and sites not imaged by both satellites were not included in the regression analysis. As a result, n=16. The rather low R^2 values signify relatively weak correlations between ice thickness and the radar measurements studied. Compared to the results for RADARSAT-2, the results for ALOS PALSAR are better except for in the HV/HH and HV/VV polarization combinations. The results presented in Figure 6a relate to regressions that include data points associated with columnar ice (9), frazil / snow ice (5), and consolidated ice (2). The latter ice type is characterized by extreme thicknesses (i.e. 145 cm and 175 cm; cf. Figure 2) and, as shown in Figure 3, generates very large radar return signals. As such, inclusion of these two data points leads to more favourable R^2 values. Figure 6b shows the results of linear regression when data points for consolidated ice are excluded. As expected, the R^2 values are reduced relative to those in Figure 6a. More importantly, the coefficients of determination for RADARSAT-2 and ALOS PALSAR are very similar. Based on the data set studied, C- and L-band SAR appear to offer similar potential for the estimation of the thickness of non-consolidated ice covers. Unfortunately, the potential appears rather limited. The effect of differences in ice structure on radar backscatter appears more important than the effect of differences in ice thickness. However, it should be noted that our data cover a quite limited range of ice thicknesses, i.e. from 70 cm to 105 cm. The availability of additional columnar and frazil / snow ice cover data points, in particular data points corresponding to lower ice thicknesses, could potentially result in improved R^2 values.

6. Concluding remarks

In this paper we have discussed the importance of radar frequency / wavelength with respect to the interaction of microwaves with river ice. We have also demonstrated the effect of frequency / wavelength on image information content through combined analysis of RADARSAT-2 (C-band) data, ALOS PALSAR (L-band) data, and ground reference data for ice covers found in the Middle Channel of the Mackenzie River at Inuvik.

RADARSAT-2 and ALOS PALSAR display a similar sensitivity to the presence of columnar ice and consolidated ice. Relative to ALOS PALSAR, RADARSAT-2 is more sensitive to the presence of frazil ice. Our data set does not include a good snow ice site and, as such, we can only hypothesize that, similarly, RADARSAT-2 will also be more sensitive to the presence of snow ice. Our simple assessment of classification potential confirms that RADARSAT-2 offers more potential for the classification of river ice types than ALOS PALSAR. HV is the best

performing linear polarisation but is surpassed by circular polarisations such as RR and LL. The even bounce component of the Pauli decomposition was found to represent a good basis for ice type classification. Further study is needed to explain this in terms of the microwave – ice interaction process.

Relative to RADARSAT-2 backscatter measurements, ALOS PALSAR backscatter measurements are found to represent a better predictor of ice cover thickness when all data points relating to columnar ice, frazil / snow ice, and consolidated ice are considered. However, a linear regression limited to data points for columnar ice and frazil / snow ice yields results that are similar for RADARSAT-2 and ALOS PALSAR. Overall, the regression results achieved are rather weak, i.e. the maximum coefficient of determination does not exceed 0.7. It should be noted, however, that the variability of our data set in terms of ice thickness is limited. More conclusive results could likely be achieved through addition of data points corresponding to lower ice thicknesses, of the order of 1 cm to 70 cm, in particular. It is expected, however, that the estimation of ice cover thickness from radar measurements will always be complicated by the strong effect of ice structural differences on the radar backscatter.

Acknowledgments

This study was made possible with the generous support of the Government of Canada Program for IPY, the Government Related Initiatives Program of the Canadian Space Agency, and the Polar Continental Shelf Program of Natural Resources Canada. The authors would like to acknowledge the contributions from the Aurora Research Institute in Inuvik (logistical support), Mr. Charles Talbot (Environment Canada, fieldwork assistance), Dr. Spiros Beltaos (Environment Canada, river ice expertise), Prof. Dr. Faye Hicks (University of Alberta, river ice expertise), and Dr. François Charbonneau (Canada Centre for Remote Sensing, MATLAB code). The ESS Contribution Number associated with this paper is 2011XXXX.

References

Duguay, C.R., T.J. Pultz, P.M. Lafleur, and D. Drai, 2002. "RADARSAT backscatter characteristics of ice growing on shallow sub-arctic lakes, Churchill, Manitoba, Canada", Hydrological Processes, Vol. 16, No. 8, pp. 1631-1644.

Fung, A.K. (1994). *Microwave scattering and emission models and their applications*. Boston, Artech House, Inc., 573 p.

Geldsetzer, T., J.J. van der Sanden, and H. Drouin. (2011). "Advanced SAR applications for Canada's river an lake ice", In: *Proceedings International Geoscience and Remoter Sensing Symposium 2011 - 'Beyond our Frontiers: Expanding our Knowledge of the World'*, Vancouver, Canada, 24 - 29 July 2011, Vol. pp. 3168-3170.

Gherboudj, I., M. Bernier, F. Hicks, and R. Leconte. (2007). "Physical characterization of air inclusions in river ice", *Cold Regions Science and Technology*, Vol. 49, No. 3, pp. 179-194.

Gherboudj, I., M. Bernier, and R. Leconte. (2010). "A backscatter modeling for river ice: analysis and numerical results", IEEE Transactions on Geoscience and Remote Sensing, Vol. 48, No. 4, pp. 1788-1798.

Leconte, R., S. Daly, Y. Gauthier, N. Yankielun, F. Bérubé, and M. Bernier. (2009). "A controlled experiment to retrieve freshwater ice characteristics from an FM-CW radar system", *Cold Regions Science and Technology*, Vol. 55, No. 2, pp. 212-220.

Mackay, J.R., 1967. "Freeze-up and breakup prediction of the Mackenzie River, N.W.T., Canada", In: W.L.Garrison & D.F.Marble (Eds.), Quantitative Geography, Evanston, Illinois, Northwestern University, pp. 25-66.

Mätzler, C. and U. Wegmüller. (1987). "Dielectric properties of fresh-water ice at microwave frequencies", *Journal of Physics, D: Applied Physics*, Vol. 20, pp. 1623-1630.

Lee, J.S. and E. Pottier. (2009). *Polarimetric radar imaging: from basics to applications*. Boca Raton, FL etc., CRC Press, Taylor & Francis Group, 398 p.

Raney, R.K., A. Freeman, R.K. Hawkins, and R. Bamler, 1994. "A plea for radar brightness", In: Proceedings of the IGARSS 1994; Surface and Atmospheric Remote Sensing: Technologies, Data Analysis and Interpretation. IEEE, Pasadena, California, 8-12 August 1994, pp. 1090-1092.

Sabins, F.F. (1996). *Remote sensing principles and interpretation. Third edition*. New York, W.H. Freeman, 3rd edition, 494 p.

Sherstone, D.A., 1984. Ice thickness in the Mackenzie Delta; winter 1982-83. Data obtained from hot-wire gauge system. Inuvik, N.W.T., Inuvik Scientific Resource Centre, 84-1, 16 p.

Sherstone, D.A., 1986. Ice thickness in the Mackenzie Delta; winter 1985-86. Inuvik, N.W.T., Inuvik Scientific Resource Centre, 86-1, 15 p.

Skolnik, M.I. (1980). *Introduction to radar systems.* New York etc., McGraw-Hill, Inc., 2nd edition, 581 p.

Terroux, A.C.D, D.A. Sherstone, T.D. Kent, J.C. Anderson, S.C. Bigras, and L.A. Kriwoken, 1981. Ice regime of the Lower Mackenzie River and Mackenzie Delta. Snow and Ice Division, Environment Canada, Hull.

Ulaby, F.T., R.K. Moore, and A.K. Fung. (1981). *Microwave Remote Sensing; Active and Passive*. Vol. I, Microwave Remote Sensing Fundamentals and Radiometry. Norwood, MA, Artech House, 456 p.

Ulaby, F.T., R.K. Moore, and A.K. Fung. (1982). *Microwave Remote Sensing; Active and Passive.* Vol. II, Radar Remote Sensing and Surface Scattering and Emission Theory. Norwood, MA, Artech House, pp. 457-1064.

van der Sanden, J.J. and H. Drouin. (2011). "Polarimetric RADARSAT-2 for river freeze-up monitoring; preliminary results", In: *Proceedings of the 5th International Workshop on Science and Applications of SAR Polarimetry and Polarimetric Interferometry (SP-695),* Frascati (Rome), Italy, 24-28 January 2011, 8 p.

van der Sanden, J.J., H. Drouin, F.E. Hicks, and S. Beltaos. (2009). "Potential of RADARSAT-2 for the Monitoring of River Freeze-up Processes", In: *Proceedings of the 15th Workshop on River Ice*, St. John's, NF, 15-17 June 2009, pp. 364-377.

Walter, K.M., M. Engram, C.R. Duguay, M.O. Jeffries, and F.S. Chapin III. (2008). "The potential use of synthetic aperture radar for estimating methane ebullition from Arctic lakes", Journal of the American Water Resources Association, Vol. 44, No. 2, pp. 305-315.

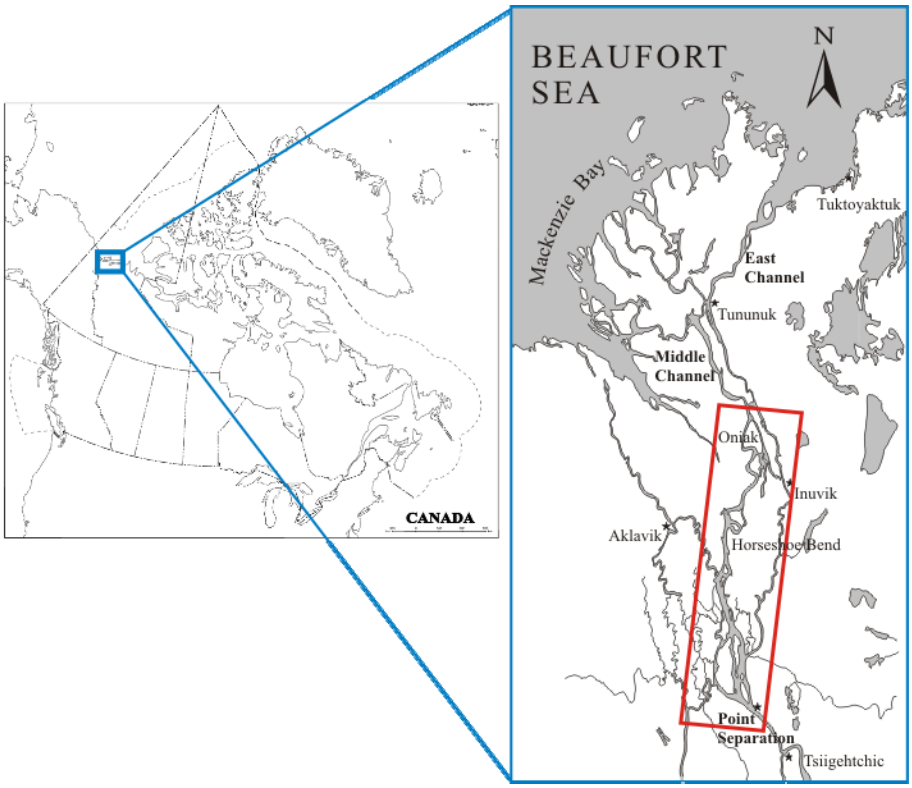

Figure 1. Maps showing the Mackenzie Delta and its location in Canada. The red rectangle identifies the main study area.

Table 1. Listing of applied SAR data.

Sensor	Local Date	Local Time	Mode	Inc. Angle
RADARSAT-2	1-Apr-09	09:35:42	Polarimetric	34.6 - 36.0
ALOS PALSAR	7-Apr-09	00:31:43	Polarimetric	22.7 – 25.0

Table 2. Definition of effective roughness for the air / ice and ice / water interface in terms of h for RADARSAT-2 and ALOS PALSAR wavelengths at an incidence angle of 35°; the temperature of the ice is assumed to be -5° C (cf. Sabins, 1996). h (in cm) corresponds to the standard deviation of the surface height irregularities.

	RADARSAT-2		ALOS PALSAR	
	Air / Ice	**Ice / Water**	**Air / Ice**	**Ice / Water**
Smooth	$h < 0.27$	$h < 0.15$	$h < 1.15$	$h < 0.65$
Rough	$h > 1.54$	$h > 0.86$	$h > 6.55$	$h > 3.67$
Intermediate	$0.27 \leq h \leq 1.54$	$0.15 \leq h \leq 0.86$	$1.15 \leq h \leq 6.55$	$0.65 \leq h \leq 3.67$

Table 3. Typical scattering behaviour of a spherical particle (e.g. air bubble) in ice as a function of diameter d (in cm) for the RADARSAT-2 and ALOS PALSAR wavelengths; the temperature of the ice is assumed to be -5° C.

	RADARSAT-2	ALOS PALSAR
Raleigh	$d < 0.10$	$d < 0.42$
Optical	$d > 9.90$	$d > 42.14$
Mie	$0.10 \leq d \leq 9.90$	$0.42 \leq d \leq 42.14$

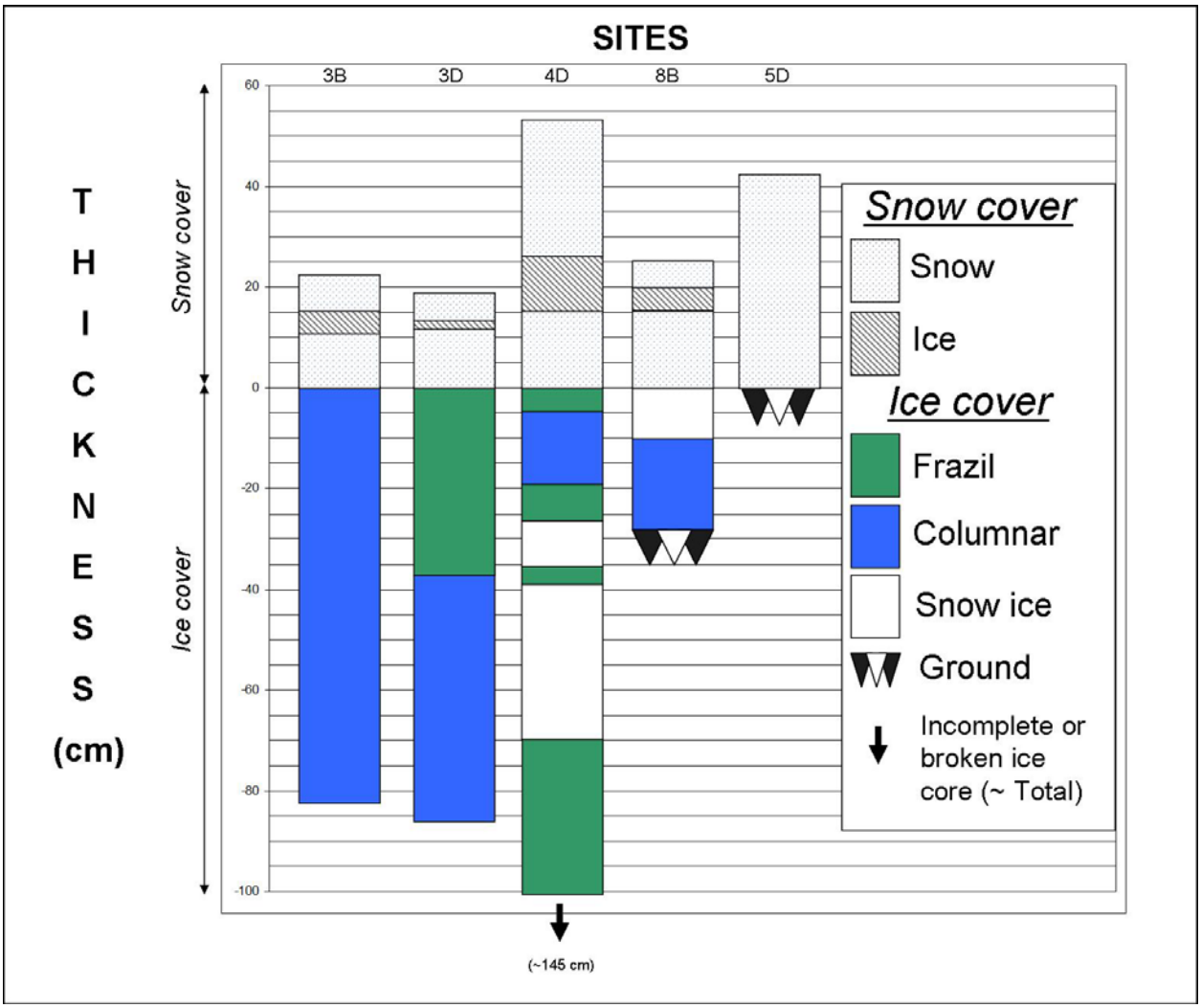

Figure 2 Graph showing the composition of the snow and ice cover at selected sites, i.e. sites the backscatter behaviour of which will be discussed in this paper. Notes: site 8-B corresponds to lake ice/snow cover; ice core 4-D only represents the upper 97 cm of a 145 cm thick consolidated ice cover.

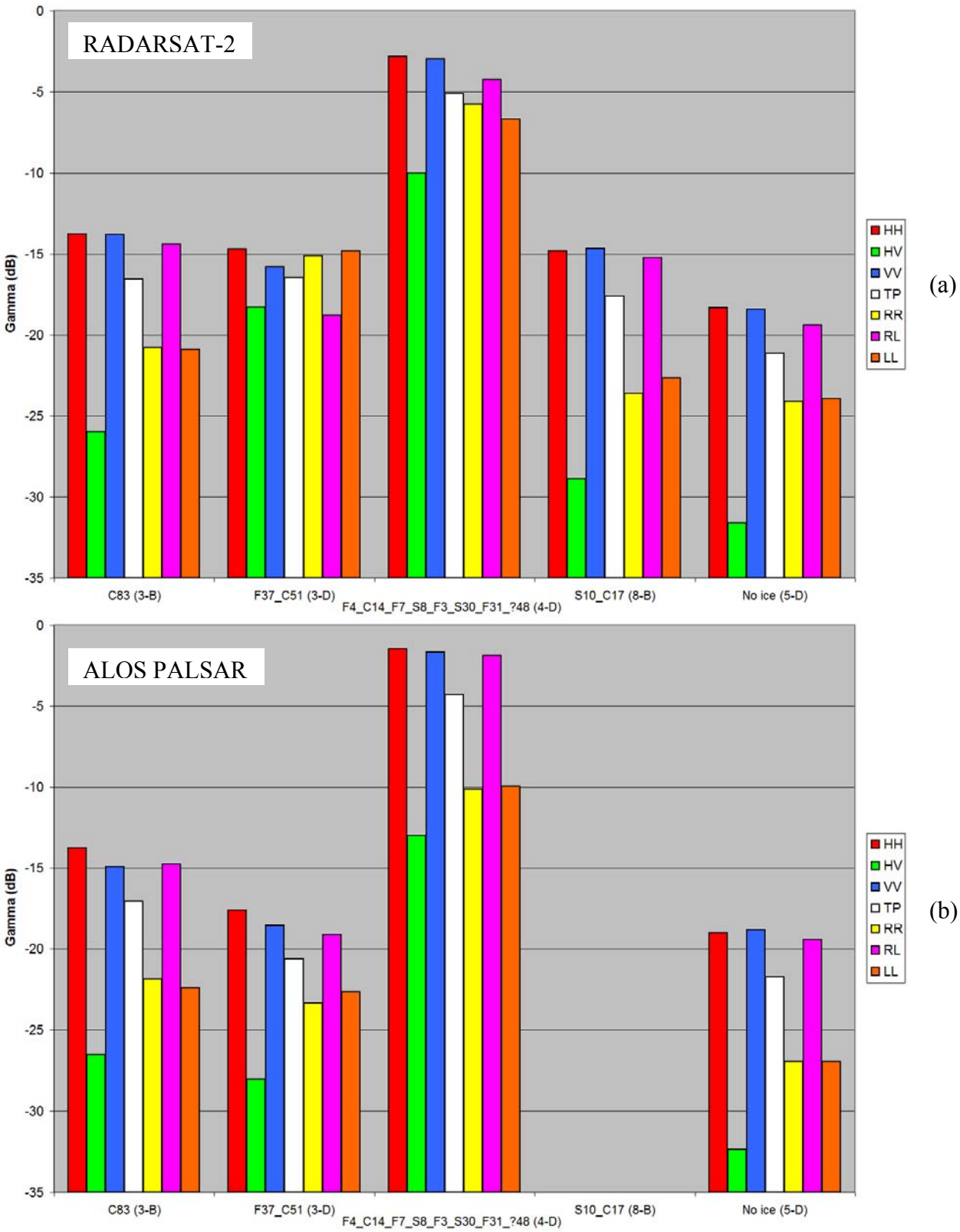

Figure 3(a-b) Radar backscatter for selected sites as a function of polarisation and frequency. (a) RADARSAT-2, C-band. (b) ALOS PALSAR, L-band.

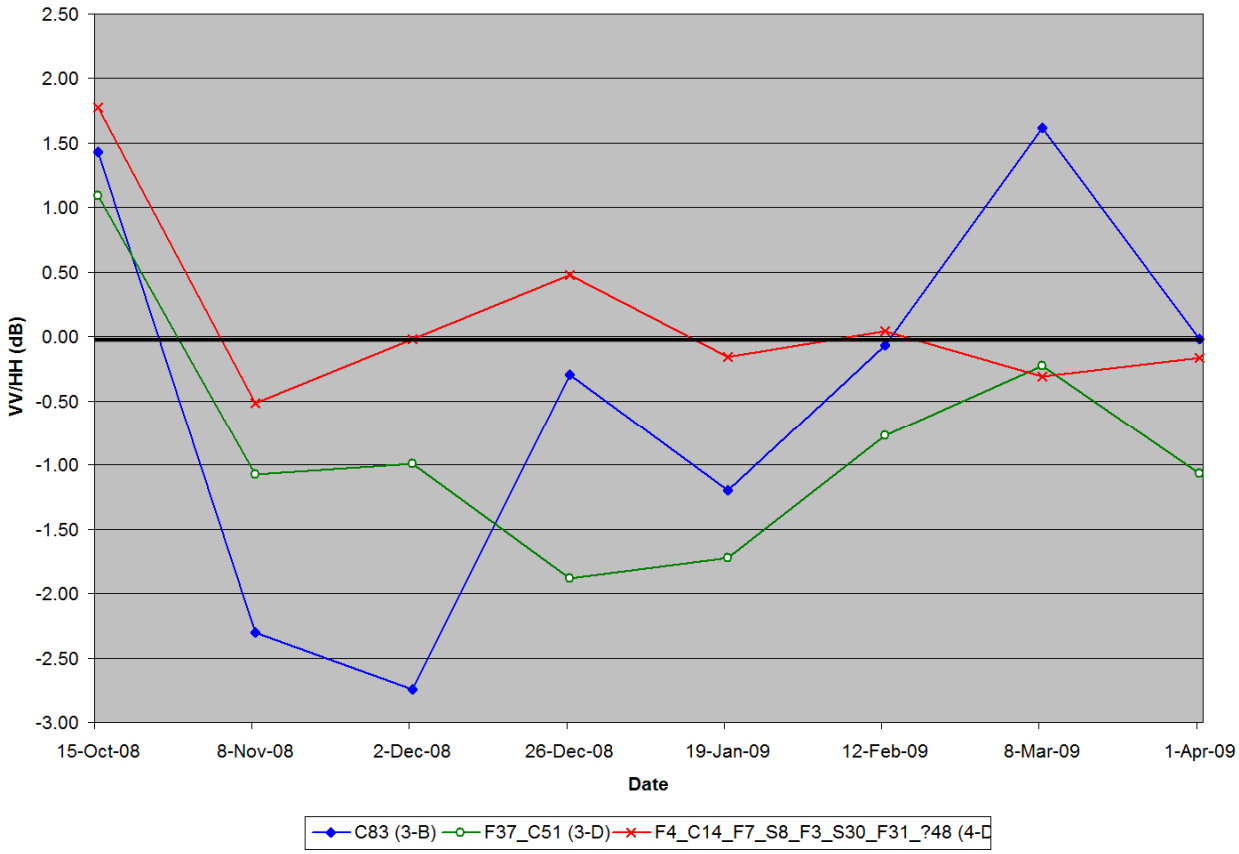

Figure 4 Evolution of RADARSAT-2 VV-HH backscatter ratio as function of time. The data points associated with October 15, 2008 correspond to open water.

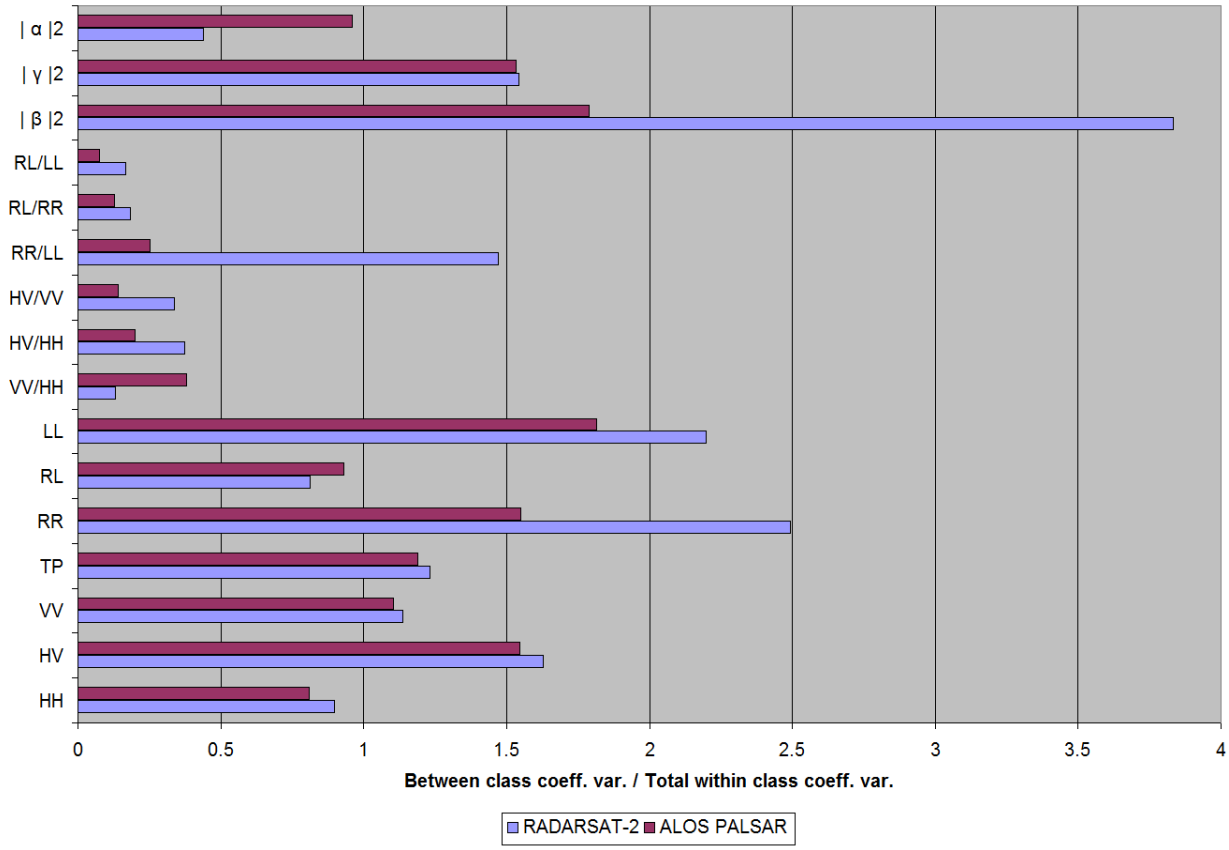

Figure 5 Relative ice cover classification potential for non-polarimetric and polarimetric variables computed from RADARSAT-2 and ALOS PALSAR.

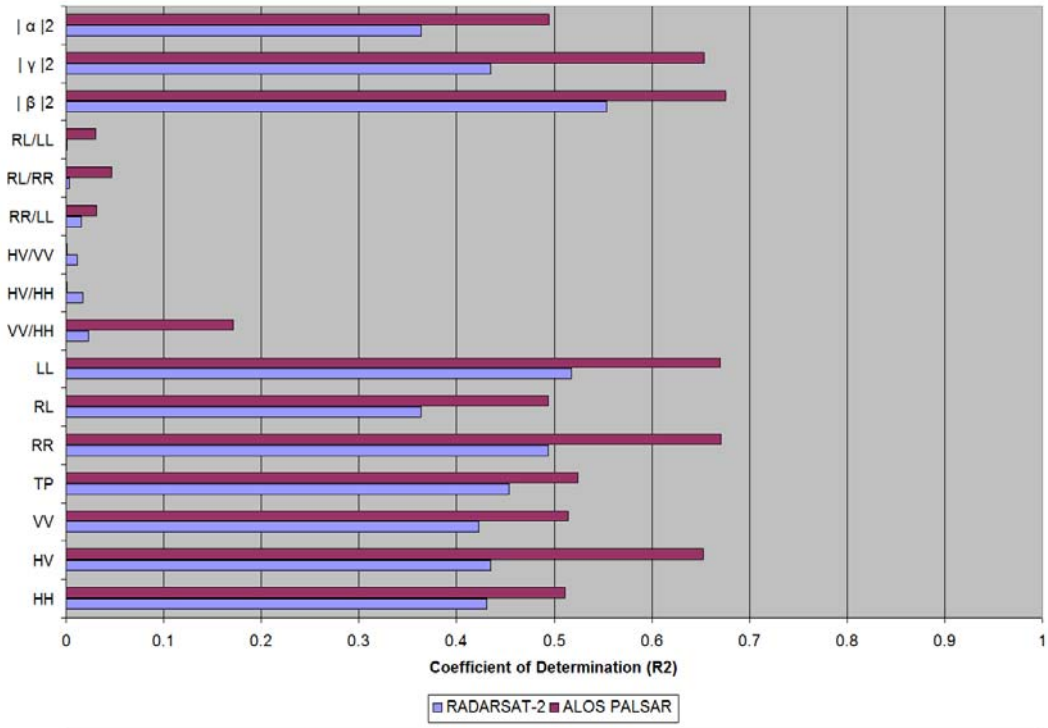

(a)

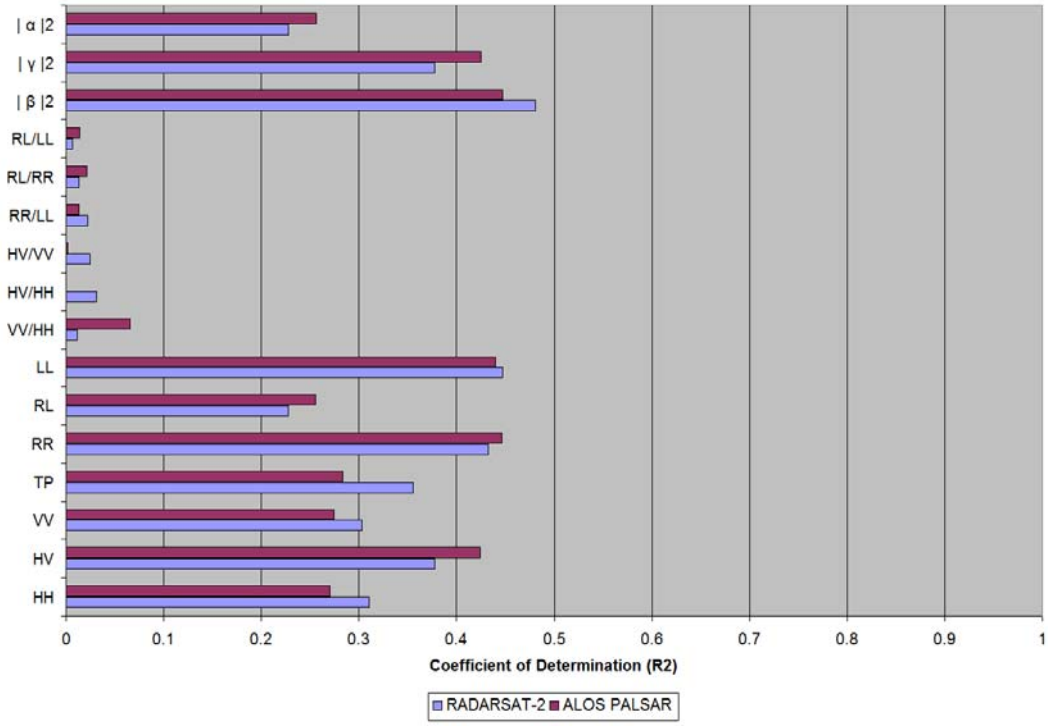

(b)

Figure 6(a-b) Relative potential for ice cover thickness estimation for RADARSAT-2 and ALOS PALSAR. (a) data points for consolidated ice included (b) data points for consolidated ice excluded.